Manuscript version: Author's Accepted Manuscript

The version presented in WRAP is the author's accepted manuscript and may differ from the published version or Version of Record.

Persistent WRAP URL:

http://wrap.warwick.ac.uk/107622

How to cite:

Please refer to published version for the most recent bibliographic citation information.
If a published version is known of, the repository item page linked to above, will contain details on accessing it.

Copyright and reuse:

The Warwick Research Archive Portal (WRAP) makes this work by researchers of the University of Warwick available open access under the following conditions.

Copyright © and all moral rights to the version of the paper presented here belong to the individual author(s) and/or other copyright owners. To the extent reasonable and practicable the material made available in WRAP has been checked for eligibility before being made available.

Copies of full items can be used for personal research or study, educational, or not-for-profit purposes without prior permission or charge. Provided that the authors, title and full bibliographic details are credited, a hyperlink and/or URL is given for the original metadata page and the content is not changed in any way.

Publisher's statement:

Please refer to the repository item page, publisher's statement section, for further information.
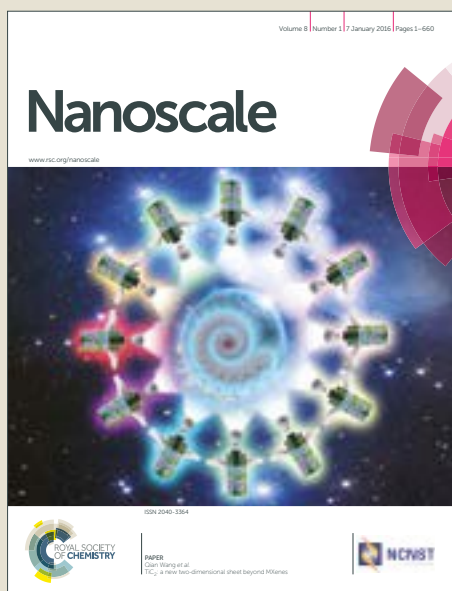
For more information, please contact the WRAP Team at: wrap@warwick.ac.uk.

warwick.ac.uk/lib-publications

Nanoscale

Accepted Manuscript

Volume 8 | Number 1 | 7 January 2016 | Pages 1–660

Nanoscale

www.rsc.org/nanoscale

ISSN 2040-3364

PAPER
Qian Wang et al.
Ti₂C₂: a new two-dimensional sheet beyond MXenes

ROYAL SOCIETY OF CHEMISTRY

NCNST

ROYAL SOCIETY OF CHEMISTRY

rsc.li/nanoscale

Facile Silane Functionalization of Graphene Oxide

Syeda S. Abbas[1], Gregory J. Rees[2], Nicole L. Kelly[2], Claire E.J. Dancer[1], John V. Hanna[2], Tony McNally[1]*

[1]International Institute for Nanocomposites Manufacturing (IINM), WMG and [2]Department of Physics, University of Warwick, Coventry, CV4 7AL UK

*Corresponding Author. E-mail: t.mcnally@warwick.ac.uk (Tony McNally)

Telephone: 0044 (0)24 7657 3256

The facile silane functionalization of graphene oxide (GO) was achieved yielding vinyltrimethoxysilane-reduced graphene oxide (VTMOS-rGO) nanospheres located in the inter-layer spacing between rGO sheets *via* an acid-base reaction using aqueous media. The successful grafting of the silane agent with pendant vinyl groups to rGO was confirmed by a combination of Fourier-transform infrared (FTIR), Raman spectroscopy, X-ray photoelectron spectroscopy (XPS) and X-ray diffraction (XRD). The structure and speciation of the silane-graphene network (nanosphere) and, the presence of free vinyl groups verified from solid-state magic angle spinning (MAS) and solution ^{13}C and ^{29}Si nuclear magnetic resonance (NMR) measurements. Evidence from Scanning Electron Microscopy (SEM), High-Resolution Transmission Electron Microscopy (HRTEM) and TEM-High-angle annular Dark-field (TEM-HAADF) imaging showed that these silane networks aided the exfoliation of the rGO layers preventing

1

agglomeration, the interlayer spacing increased by 10Å. The thermal stability (TGA/DTA) of VTMOS-rGO was significantly improved relative to GO, displaying just one degradation process for the silane network some 300 ^{o}C higher than either VTMOS or GO alone. The reduction of GO to VTMOS-rGO induced sp^2 hybridization and enhanced the electrical conductivity of GO by 10^5 Sm^{-1}.

KEYWORDS: reduced graphene oxide (rGO), vinytrimethoxysilane (VTMOS), functionalization; silane nanospheres, covalent grafting

1. Introduction

Graphene, an allotrope of carbon, is a monolayer of sp^2 hybridized carbon atoms in a two dimensional lattice and continues to gain intense attention due to its extraordinary intrinsic properties. These include high surface area (>2600 m^2/g)[1], exceptional thermal conductivity, (~3000 W m^{-1} K^{-1})[2] mechanical properties (Young's modulus of 1.0 TPa)[3-5], electrical conductivity (2 x 10^3 S cm^{-1})[6] and 97.7% optical transparency[7-8]. The structure of graphene is that of a densely packed honeycomb structure of individual layers, characterised through single-crystal X-ray crystallography. As the atoms of the carbon form strong covalent bonds throughout the honeycomb lattice, the strength to weight ratio outweighs all metals and metal composites. Regardless of its high strength, it is still relatively flexible and can be wrapped up into 0-D fullerenes, rolled into 1-D nanotubes or stacked in a 3-D graphite[9]. Due to its exceptional properties, it can be used for a wide range of applications as diverse as transparent conductive electrodes[10], energy storage devices[11], for biomedical purposes such as drug delivery[12], cancer therapy[13] and can be incorporated into polymer matrices as a functional filler[14].

For composites of graphene and polymers, full translation of properties from the graphene to the polymer matrix is highly dependent on the extent of dispersion and distribution of the graphene layers within the polymer matrix and the interfacial interaction between these two phases. Agglomerates of graphene are formed from a combination of high surface area, strong van der Waals interactions and π-π bonding between layers which makes them insoluble in organic polymers[15]. Therefore, it is essential to modify graphene with functional groups to increase compatibility between the graphene and polymer matrix and to promote interfacial interactions.

Graphene Oxide (GO) can be homogenously dispersed in water and other polar media due to its various carbonyl and other polar moieties present on the basal planes and edges[16-17]. These functional groups are available as reactive sites for further functionalization. Recently, silane coupling agents have been employed as compatibilizers for nanofillers and polymers promoting interfacial interactions. These silane coupling agents consist of organosilanes, $(R_1, R_2, R_3)SiX_n$, where X substituents are hydrolysable to form $RSi(OH)_3$ when reacted with water, whereas the R groups are usually unreactive[18]. Different silane agents such as aminopropyltriethoxy silane (APTES)[19-24], triethoxymethoxysilane (MTES), 3-glycidyloxypropyl trimethoxysilane (GPTMS)[25-27] and triethoxysilane (TEOS)[28-30], have been widely explored and investigated for GO functionalization. However, to the best of our knowledge no studies have been reported that have focused on using vinyltrimethoxysilane (VTMOS) to modify reduced GO (rGO). VTMOS has three hydrolysable methoxy groups and one vinyl group attached to silicon. Ma *et al.* functionalized GO using VTMOS *via* ultrasonication to incorporate GO into a silicone matrix by solvent mixing[25]. The mechanical properties and thermal stability of this matrix was improved significantly with very low GO loadings. The enhancement in properties was due to the vinyl

group of the silane agent reacting with the silicone matrix facilitating interfacial interactions. Additionally, Wang *et al.* modified GO with vinyltriethoxy silane (VTES) in acidic conditions and then reduced the GO using hydrazine/ammonia prior to inclusion in a LDPE matrix *via* solvent mixing to investigate mechanical and barrier properties of the nano-composite[26]. The method used to silanise graphene included the use of water as a solvent medium. However, in both papers, the functionalized graphene obtained was not characterized to a level that unequivocally confirmed functionalization of the graphene network. In this work 'nanoballs', spherical particles with diameters in the range 10-30nm were produced from VTES and although observed by TEM, they were not further characterized. The 'nanoballs' produced were actually silsesquioxane nanoparticles obtained from the hydrolysis/condensation reactions aided by acidic and basic conditions. These silica spheres were first produced by Stöber[31] in 1968 and widely investigated in the last decade. This method involved a silane precursor, usually tetraethoxysilane (TEOS) in a mixture of water, ammonia and alcohol. To modify these silica particles with different functional groups, mixtures of TEOS and organotrialkoxysilane precursors can be utilized. More than one starting precursor is usually used and the experiment becomes more complex with the need to manage ratios of the ethanol:water solvent medium.

In contrast, in the experimental procedure described in our work, only one silane precursor was used in a water medium to form silica-nanospheres. In this study, GO was modified by VTMOS using acidic conditions and then reduced using hydrazine, providing the silane agent acidic and basic conditions for the hydrolysis/condensation reactions to form silane nanospheres. Therefore, we report a facile route to synthesise VTMOS-rGO which was then studied in detail using microscopic methods such as TEM and TEM-HAADF and SEM, and the chemical and surface composition determined using FTIR, XPS, XRD and Raman spectroscopy. Additionally, solid

state ^{13}C and ^{29}Si MAS NMR and solution state NMR studies were undertaken to analyse the speciation defining these systems. DC measurements and thermal properties were measured using a two-point probe method and TGA, respectively. To the best of our knowledge, this is the first study using this method to produce VTMOS-rGO silica nanospheres, a silane-graphene network and characterized in detail. This facile methodology can be expected to provide well controlled modified graphene(s) which can thereby enhance interfacial interactions with any polymer matrix of interest during melt mixing.

2. Experimental

Materials: GO (1 nm thick/ size of flakes 2-20μm) was purchased from Abalonyx, VTMOS (98%) from Alfa Aesar, hydrazine yydrate (78-82%) and ammonia solution (2M in methanol) were purchased from Honeywell Fluka and, Hydrochloric acid (37%) from Fisher Chemical.

VTMOS-rGO. For modification of GO, GO powder was added to a mixture of diluted HCl (0.40 M) and VTMOS and heated for 2 hours at 75°C. Modified GO dissolved in water and formed a dark brown solution. This solution precipitated out when the hydrazine/ammonia mixture was added and the mixture was heated for another 4 hours at 90°C under reflux. After the acquired time, this mixture was then filtered and washed off with water, ensuring that the sample had a neutral pH and, dried off in a vacuum oven. For comparison, VTMOS-GO was also prepared using the same method but dried in a freeze dryer.

Characterization. Scanning Electron Microscopy (SEM) micrographs were obtained using a Zeiss Sigma using InLens detector at 5kV. The samples imaged were sputter coated using an Au/Pd target. Transmission Electron Microscopy (TEM) micrographs were obtained using a Talos (FEI) F200X for TEM/STEM with Super-X EDS operated at 200kV for both TEM and

STEM elemental mapping. Samples for TEM analysis were prepared *via* drop-casting a few milliliters of sample dispersions after ultrasonication onto holey carbon grids, allowing the solvent evaporate and leaving the sample to rest for 24 hours at RT.

Fourier-transform infrared (FTIR) spectra were recorded on a Bruker Spectrometer with a scan range from 500 cm^{-1} to 4000 cm^{-1}.

X-ray Diffraction (XRD) measurements were completed on a Panalytical Empyrean instrument in Bragg-Brentano geometry with Co-K$_\alpha$ radiation (1.7903 Å) and a solid state Pixcel detector for fast data collection. A variable divergence slit was used to control the size of the beam on the sample to be 6mm parallel to the beam and a beam mask of 15mm. 20 minute scans were collected in the range 4 – 40° 2θ with a step size of ~ 0.026 ° 2θ.

Raman Spectra were recorded on a Renishaw inVia Reflex Raman Microscope with a 532 nm excitation source and a 100X microscope objective. Samples were in pellet form.

X-ray Photoelectron Spectroscopy (XPS) was carried out using a Kratos Axis Ultra DLD Spectrometer at RT and with a base pressure of 2 x 10^{-10} mbar, using a monochromated Al k$_\alpha$ X-ray source. In order to prevent surface charging, the data was collected while the sample was exposed to a flux of low energy electrons from the charge neutralizer built in to the hemispherical analyser entrance, with the binding energy scale retrospectively calibrated to the sp^3 C-C peak at 284.6 eV. The data was analyzed with the CasaXPS package, using Shirley backgrounds and mixed Gaussian-Lorentzian (Voigt) line shapes and asymmetry parameters where appropriate. For compositional analysis, the analyser transmission function was determined using clean metallic foils to determine the detection efficiency across the full binding energy range.

All solid-state ^{13}C magic-angle-spinning (MAS) nuclear magnetic resonance (NMR) spectra were acquired at 7.05 T using a Bruker Avance HD-300 spectrometer operating at ^{1}H and ^{13}C Larmor frequencies (ν_0) of 300.13 MHz and 75.8 MHz, respectively. A Bruker 4 mm dual channel HX MAS probe was utilized to enable MAS frequencies (ν_r) of ~12 kHz for all measurements. Single pulse experiments were employed where a $^{\pi}/_2$ excitation pulse of 4μs duration was implemented in conjunction with 100 kHz of ^{1}H decoupling which was applied during acquisition, and the recycle delay was 10 s. The ^{13}C MAS NMR data were chemical shift referenced (indirectly) to neat TMS (δ_{iso} = 0.0 ppm) via an alanine secondary (solid) reference which yields three distinct resonances for the methyl, backbone and carbonyl carbon species (δ_{iso} = 20.5, 50.5 and 178 ppm with respect to TMS, respectively).

Corresponding ^{29}Si MAS NMR data were also measured at 7.05 T (Larmor frequency ν_0 = 59.59 MHz) on a Bruker Avance HD-300 Spectrometer. A Bruker 7 mm dual channel HX MAS probe was utilized to facilitate MAS frequencies (ν_r) of ~5 kHz for all measurements. The single pulse experiments consisted of a $^{\pi}/_2$ excitation pulse of 4.0 μs duration, 100 kHz of ^{1}H decoupling during acquisition, and a measured recycle delay of 10s. All ^{29}Si chemical shifts were indirectly referenced to TMS (δ_{iso} = 0.0 ppm) via a kaolinite secondary (solid) reference (δ_{iso} = −93 ppm with respect to TMS), and the ^{29}Si pulse length calibration was undertaken on the kaolinite secondary reference.

Both ^{13}C and ^{29}Si solution state NMR experiments were performed at 7.05 T in a Bruker 7 mm MAS NMR probe; the excitation pulse parameters mirrored those implemented in the solid experiments, however no ^{1}H decoupling or magic angle spinning were utilized.

Thermogravimetric Analysis (TGA) was carried out using a Mettler Toledo thermal analyzer over the temperature range of 25°C to 800°C at a heating rate of 10 °K/min under nitrogen.

Electrical conductivity measurements were performed using a two-point probe method on hydraulic pressed pellets. An electrometer (Keithley, Ohio, USA, model 6517B) was used to measure the volume resistivity using an applied voltage of 1V.

3. Results and Discussion

The synthetic route to produce VTMOS-rGO is divided into two major steps, see Scheme **1**. The first step shows the addition of the silane agent in acidic conditions which encourages the simultaneous hydrolysis of the O-Me groups in VTMOS and the grafting with GO *via* OH groups through a condensation reaction.
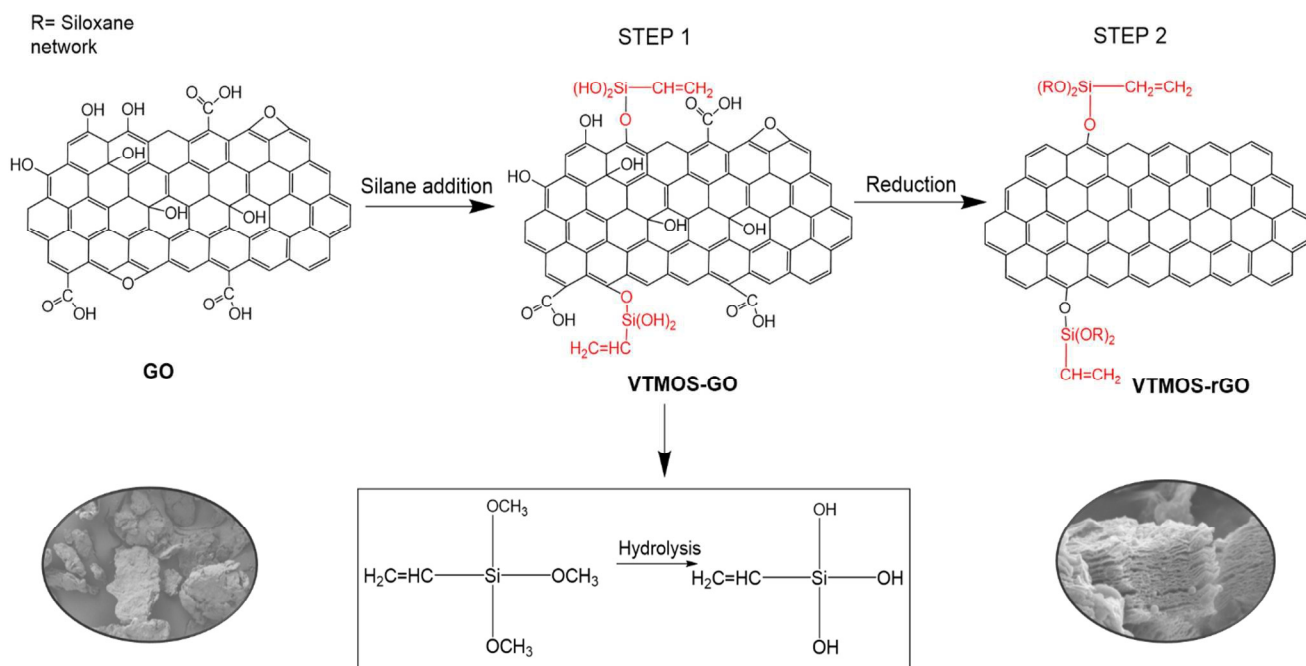
Scheme 1: Schematic representation of the modification of GO. SEM image (left): magnification x 700k), Step 1: silane addition and Step 2: reduction of silane modified GO. SEM image (right): magnification x 50k)

This acid-catalyzed hydrolysis yields a rapid protonation of the methoxy group followed by a S_N2-type displacement of the leaving group by water as illustrated in Scheme 2. This step yields a brown solution that precipitates and turns black when the pH was increased in the second step after the addition of hydrazine/ammonia. The reducing agent partially retains π-π conjugation. The second step can proceed by two different routes. Route 1 follows the self-condensation reaction to form poly(siloxane) bonds, whereas route 2 results in the formation of siloxane bonds *via* nucleophilic attack of the amine followed by rapid attack of neighbouring silanols.

Step 1

Step 2
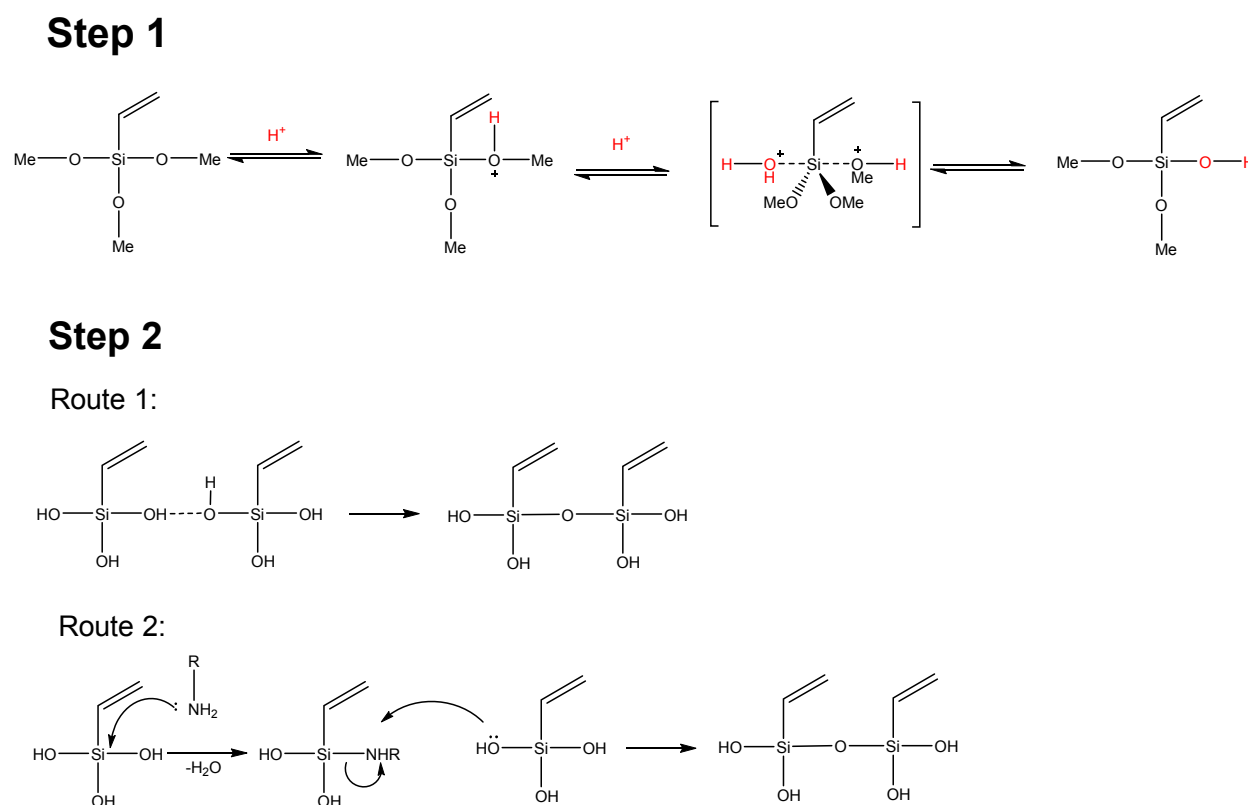
Route 1:

Route 2:

Scheme 2. Reaction mechanisms for step 1 and step 2, (two possible routes).

The concept of amines acting as nucleophiles was supported by the work of Chojnowoski and Chrzczonowicz who demonstrated that condensation reactions could also be catalyzed by

secondary and tertiary amines *via* nucleophilic attack on the silicon[28]. The polycondensation pathway is dependent on the functional groups attached and can result in different reactivities. Differences in reactivity may be caused by steric hindrance associated with these functional groups and the type of intramolecular interactions caused between ring systems. Steric hindrance causes straight chains to form rings rather than branched chains to form further chains. When two poly(silanol) rings are in close proximity strong hydrogen bonding can be formed to yield micro-spheres, which are evident from SEM and TEM images (see Figure 1 and Figure)[32].
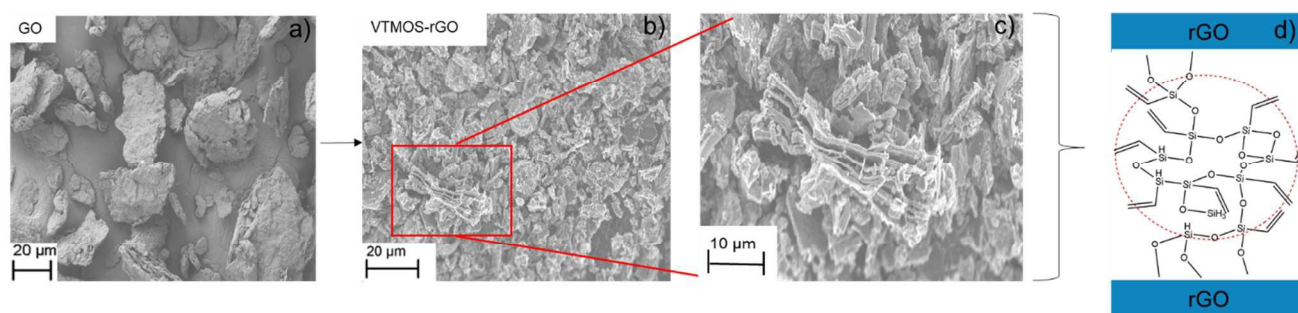

Figure 1. SEM images showing GO before a) and after b) modification with VTMOS and c) is b) at higher magnification showing layers of rGO exfoliated with silane spheres. The silane-sphere network formed is illustrated diagrammatically in d).
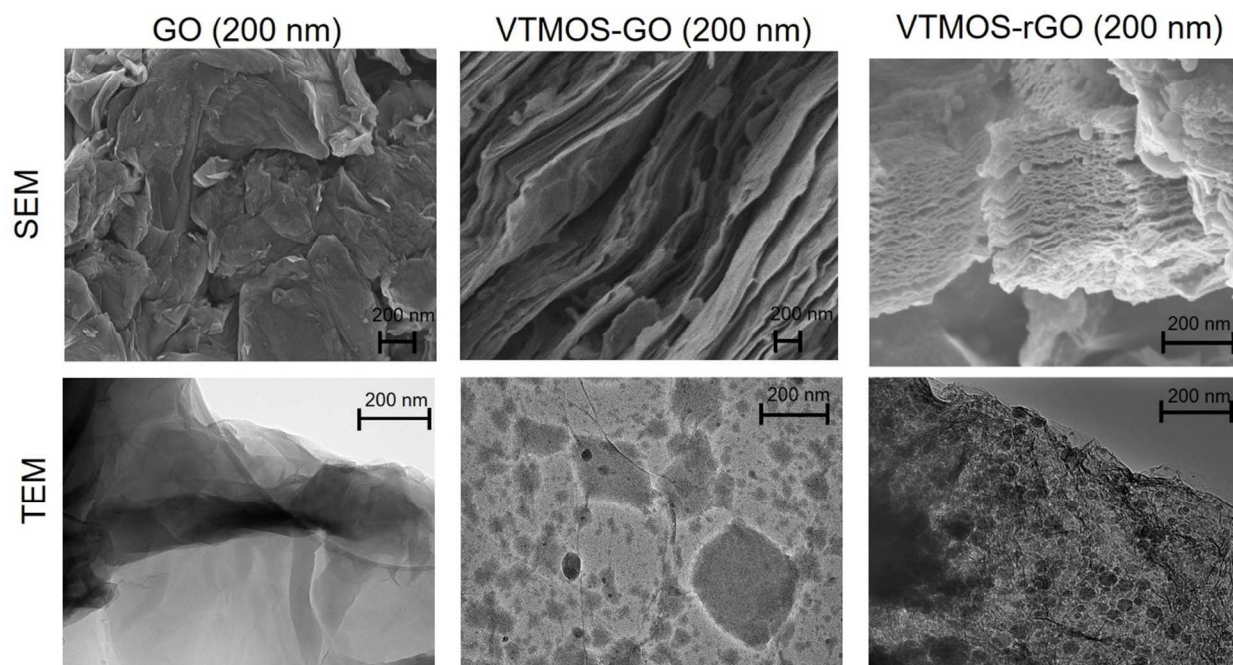
Figure 2. SEM and TEM images of GO, VTMOS-GO and VTMOS-rGO at different magnifications, clearly showing the silica nano-spheres located in the interlayer spacing of rGO.

The nanospheres are uniform in shape but not monodisperse, having diameters typically in the range 10nm to 500nm. The basic conditions promote self-condensation of the silanols to form siloxane networks to yield spherical structures, i.e. silane nanospheres readily observed in the SEM and TEM images of VTMOS-rGO but not for VTMOS-GO. Furthermore, it can be seen that the silane spheres are distributed between the rGO layers which induces exfoliation. Grafting with the silane forms uniform spheres located mainly within the rGO interlayer spacing and is expected to prevent agglomeration of these layers when later mixed with polymers. Moreover, in previous studies[33-35], silica spheres were formed either by using TEOS or a mixture of silane precursors that aided the nucleation of silica spheres. Instead of using various silane precursors, Hay *et al*[35] used a sodium silicate solution as a seed for further growth of silica spheres. Whereas in this study, it can be seen from the SEM images, that graphene sheets provide sites for silica sphere formation and act as seeds (Figure 2). From the TEM images in Figure 2, the few layer

GO is transparent with a wrinkled structure, whereas the structure of VTMOS-rGO shows an even distribution of the nano-spheres on the surface and between rGO layers, verified with elemental analysis (Figure 3). Figure 3 shows EDS elemental mapping of carbon, oxygen and silicon in red, blue and green, respectively. These images confirm the presence of the silane nanospheres causing exfoliation of the rGO layers. After modification, the layers of rGO were well-separated with silane nanospheres located in the inter-gallery spaces.
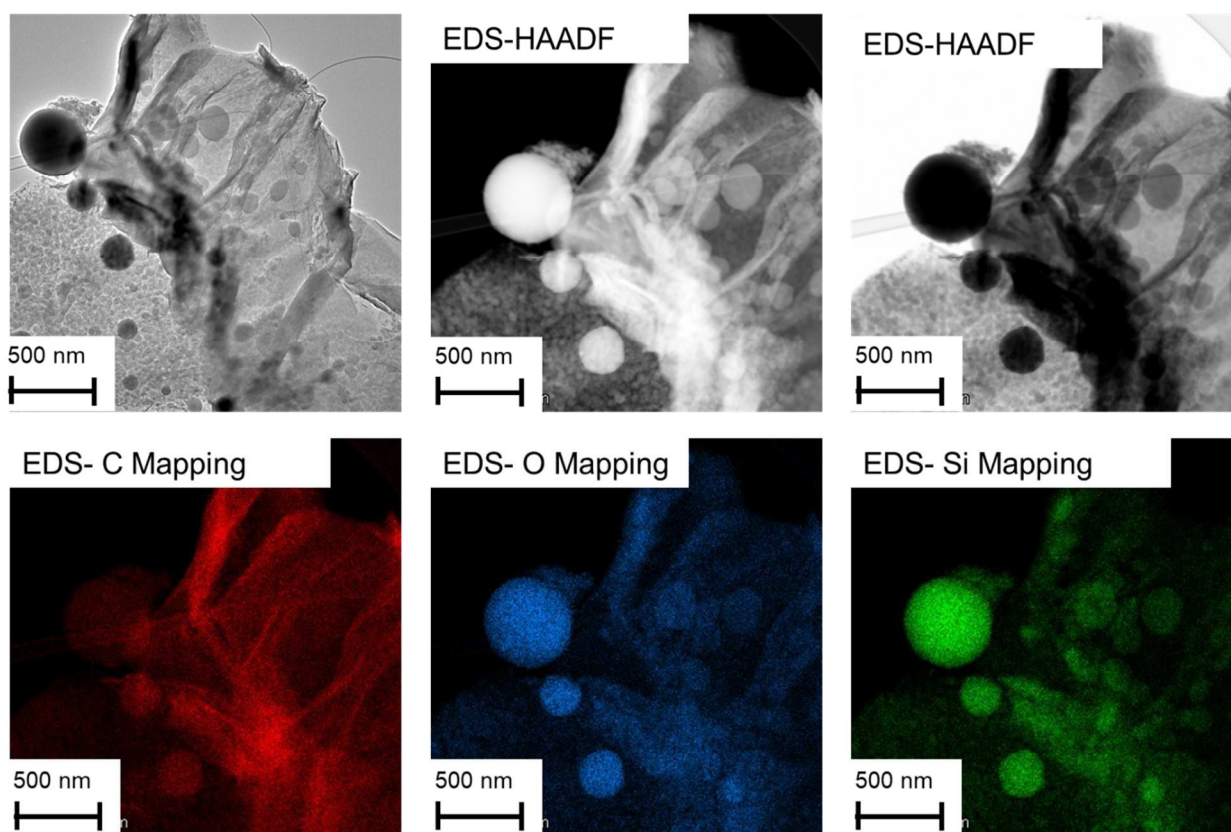

Figure 3. TEM-EDS HAADF images of VTMOS-rGO. Elemental mapping showing carbon (red), oxygen (blue) and silicon (green). Each map is independent of its own maximum intensity.

To confirm covalent bonding of the silane agent to the rGO, FTIR spectra of the precursors and VTMOS-rGO were collected (Figure 4). The FTIR spectrum of GO has a broad band

12

associated with the hydroxyl groups between 2874-3678 cm^{-1}. Additionally, other peaks at 1720 cm^{-1}, 1612 cm^{-1} and 1035 cm^{-1} corresponded to carbonyl (C=O stretching), aromatics (C=C) and epoxy groups (C-O-C), respectively. The FTIR spectrum of pure VTMOS was also recorded and contains bands derived from methoxy groups at 1188 cm^{-1} and 1078 cm^{-1}, and vinyl group at 1008 cm^{-1} and 966 cm^{-1} [36-37]. For VTMOS-GO, the peaks corresponding to the hydroxyl (2892-3690 cm^{-1}) and the carbonyl groups (1608-1730 cm^{-1}) remained, with extra peaks for the Si-O-C (1016 cm^{-1}) bond and the Si-O-Si (1109 cm^{-1}) vibration obtained. In the FTIR spectrum of VTMOS-rGO, the broad band derived from the hydroxyl groups in GO had disappeared for this sample due to complete reduction, relative to VTMOS-GO. Furthermore, the epoxy groups on the GO (peak at 1035 cm^{-1}) were reduced by hydrazine and used for grafting to the silane agent and, a new peak evolved at 1026 cm^{-1} corresponding to Si-O-C bonding. Additionally, the peak at 1087 cm^{-1} corresponds to Si-O-Si vibrations, evidence for the hydrolysis of the methoxy groups to OH groups on the silane agent that then formed siloxane networks under basic conditions (Si-O-Si). Furthermore, the presence of Si-O-C bonds confirms the successful grafting of rGO with the silane agent through hydroxyl functionality. These results confirm the complete reduction of GO to rGO and grafting of the siloxane network to the surface of rGO. The peaks at 995/958 cm^{-1} are from free unreacted vinyl groups present.
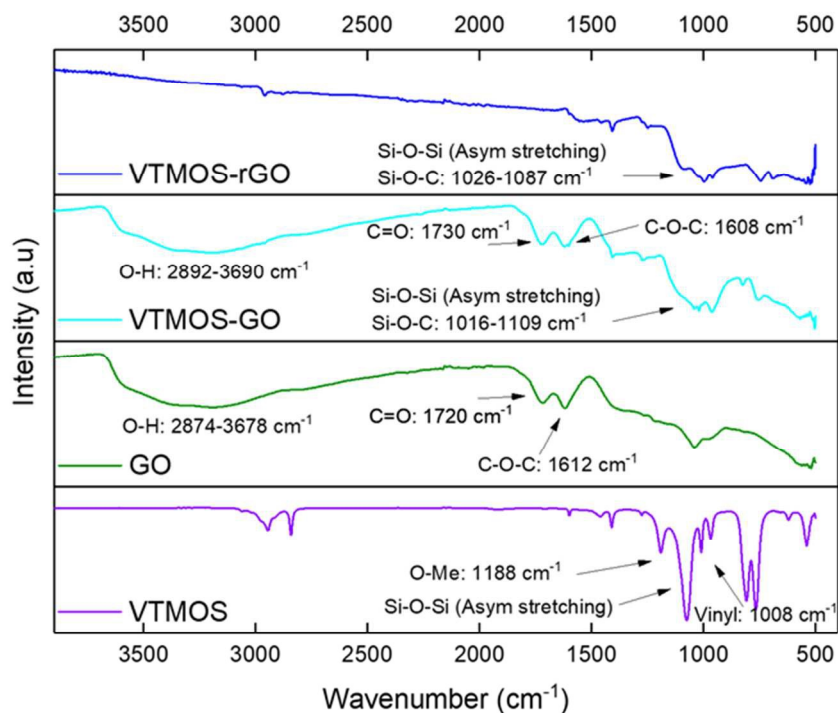
Figure 4. FTIR spectra of VTMOS-rGO, VTMOS-GO, GO and VTMOS.

XRD was used to determine changes within the interlayer spacing of GO and crystalline properties of the samples. Using the measured diffraction angle *2θ*, the interlayer spacing *d* between the layers of graphene was calculated using Bragg's law, n*λ* = *2d.sinθ* (where *λ*= 0.1789). Figure 5 shows the XRD spectrum for GO which displays a peak at 2θ=12.20°, corresponding to an interlayer spacing of 0.84 nm. Relative to GNPs (2θ= 30.85, d-spacing: 0.37 nm[38]) the interlayer spacing for GO is significantly larger due to the presence of oxygen functionalities on the surface of GO. The different carbonyl functionalities on GO are located between the layers resulting in greater interlayer spacing. After the addition of VTMOS onto GO, the Bragg angle for 2θ=11.31° decreased and the interlayer spacing of 0.91nm increased indicating exfoliation of GO layers by VTMOS. A broad peak was also seen in the range 2θ=15-35°, related to the amorphous VTMOS grafted onto the GO.[39] Furthermore, after the addition of

the silane agent to GO and reduction, VTMOS-rGO displayed two main peaks. Firstly, a peak at $2\theta=10.90°$ corresponding to an increase in interlayer spacing up to 0.94nm due to the silane grafting successfully to rGO. The grafted silane agent hinders π-π interactions between the rGO sheets facilitating intercalation of the silane within the graphene layers. The increased interlayer distance was observed during SEM imaging (see Figure 3)[38]. The second peak at $2\theta=26.91°$, corresponding to an interlayer spacing of 0.24nm, demonstrates effective reduction of the hydroxyl groups. The breadth of this peak corresponds to the different size ranges of silica nanospheres present which cause variations in the intercalation between the graphene layers. The broad peak is also associated with amorphous silica structure at 23.6°[40]. These results confirm the successful grafting and presence of the silane cross-linked network between the rGO layers.
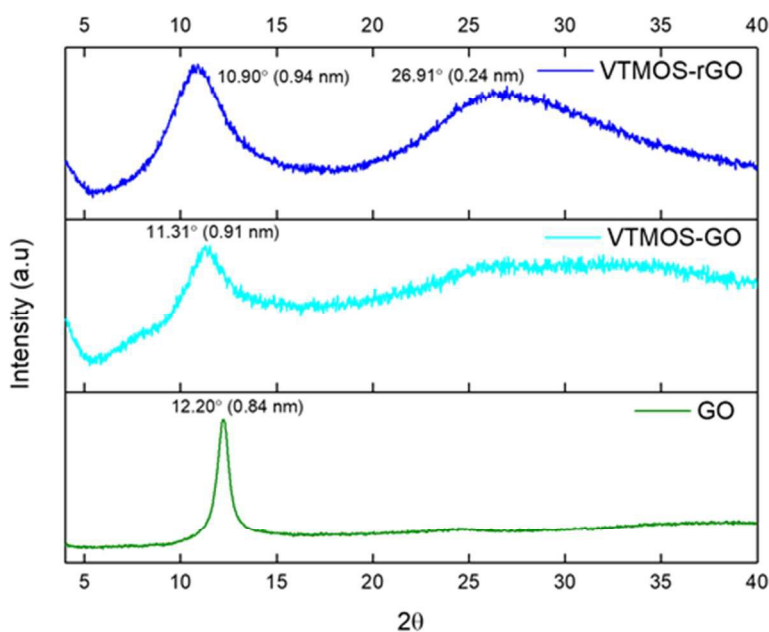

Figure 5. XRD patterns of VTMOS-rGO, VTMOS-GO and GO.

The Raman spectrum of graphene classically displays two main peaks, the G band (at 1581 cm^{-1}) and a second overtone of an in-plane vibration, the D band (at 1347 cm^{-1}). The G band corresponds to sp^2 hybridisation whereas the evolution of the D band is derived from defects and

a decrease in the size of the in-plane sp^2 domains caused by oxidation[41]. For example, for graphene nanoplatelets (GNPs), there is much more sp^2 hybridisation (i.e. fewer defects). This can be seen in Figure 6 which shows a lower D band intensity relative to the G band. In contrast, for GO and VTMOS-rGO a more intense D band relative to that for GNPs was observed. The ratio of the two bands (I_D/I_G) quantifies the number of defects within the sample and is given in Table 1. As GO is reduced the G band shifts from 1595 cm^{-1} to 1590 cm^{-1}, which is similar to that for GNPs (1582 cm^{-1}), confirming some restoration of the sp^2 network[42]. As GO is functionalised with the silane cross linker, I_D/I_G increased from 0.90 to 0.91 for VTMOS-GO. Even after functionalisation, the I_D/I_G remained almost the same, implying that the covalent bonding between the VTMOS and GO sheets has been successful without much destruction to the carbon lattice[26]. This value increased for VTMOS-rGO to 1.0 confirming grafting of the silane cross-linker between the rGO layers.
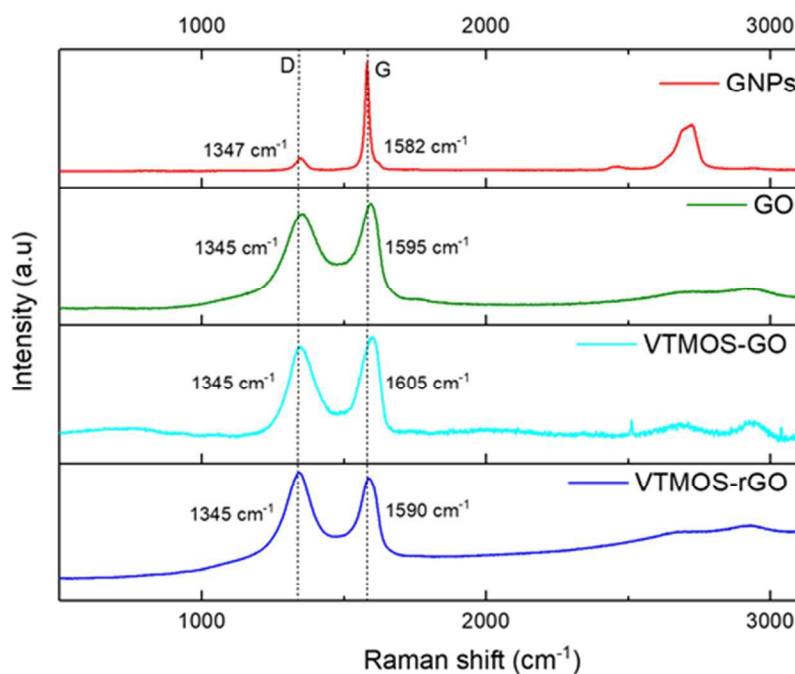

Figure 6. Raman spectra of VTMOS-rGO, VTMOS-GO, GO and GNPs.

Table 1. Wavenumber positions of the D and G bands and, the measured intensity ratio for I_D/I_G for GNPs, GO, VTMOS-GO and VTMOS-rGO

	D band (cm^{-1})	G band (cm^{-1})	$I_{D/G}$
GNPs	1347	1582	0.12
GO	1345	1595	0.90
VTMOS-rGO	1345	1605	0.91

Further evidence for the success of the silane grafting was obtained from XPS measurements, which were carried out on VTMOS-rGO and GO. As seen from the survey spectra in Figure 7 and the data in Table 2, VTMOS-rGO displays two new peaks in the XPS spectra corresponding to a silicon signal at 153.59 eV and 102.59 eV, binding energies for 2s and 2p respectively, relative to the GO spectra. The C1s spectrum was deconvoluted into seven different peaks attributed to binding energies for C-C/C-H (284.7 eV), C-O / C-O-Si (285.9 eV), C=O (287.4 eV), O=C-O (288.9 eV), sp^2 C shake-up (290.6 eV) and C-Si (283.7 eV), shown in Figure 7. The peak for C-Si reveals the presence of the vinyl group present and the C-O-Si confirms the grafting of the graphene with the nano-spheres through the carboxyl groups of the GO later reduced. This is further verified from the Si 2p spectra that shows peaks for Si-C, Si-O-C (101.9 eV) and Si-O-Si (104.6 eV) which were absent in the XPS spectrum of GO[20].

17
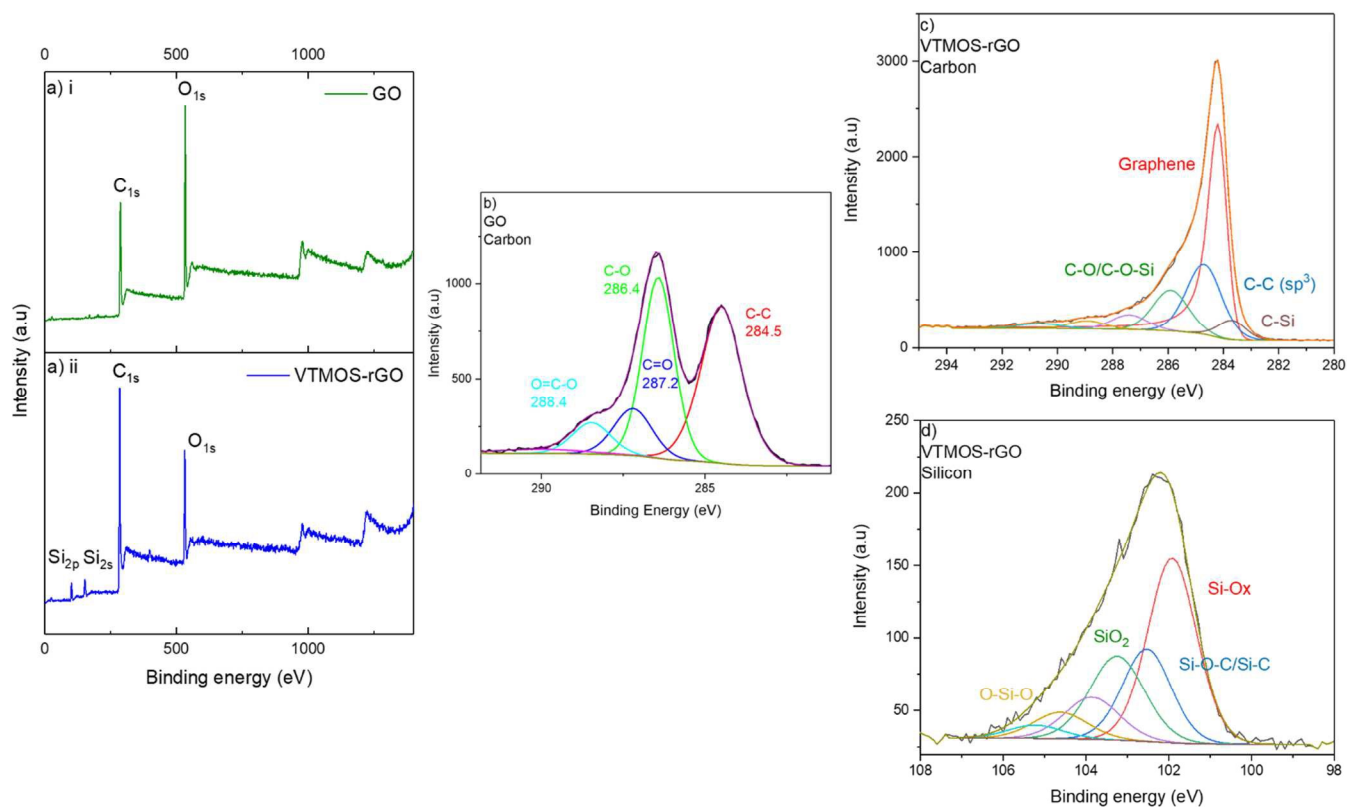
Figure 7. a) i XPS survey spectra for GO and a) ii for VTMOS-rGO and, XPS spectra for b) C1s of GO and c) C1s and d) Si 2p of VTMOS-rGO.

Table 2. Deconvoluted XPS data for C1s and O1s of GO.

	Binding energy (eV)	Atomic %	Bonding environment
C 1s	284.5	42.17	C-C
	286.43	36.3	C-O
	287.2	11.44	C=O
	288.47	7.67	O=C-O
	290.04	2.41	Shake-up feature
O 1s	531.33	11.47	O=C

18

532.31	75.62	O-C / Atm O
533.5	10.36	Atm O
535.34	2.55	H_2O

Table 3. Deconvoluted XPS data for C1s, O1s and Si2p of VTMOS-rGO.

	Binding energy (eV)	Atomic %	Bonding environment
C1s	284.2	40.39	Graphene
	284.7	26.94	C-C/C-H (sp^3)
	285.9	15.73	C-O / C-O-Si
	287.4	5.65	C=O
	288.9	3.13	O=C-O
	290.6	2.27	sp^2 C shake-up
	283.7	5.88	C-Si
O1s	530.1	5.75	O=C (aromatics)
	531.8	48.26	SiO_2/O=C/Atm O
	532.9	30.55	SiO_x/O-C/Atm O
Si 2p	101.9	59.84	Si-C/Si-O-C
	103.2	30.58	SiO_2
	104.6	9.59	O-Si(-O)-O

Combined solid-state MAS and solution ^{13}C and ^{29}Si NMR were undertaken to confirm the

bonding arrangement of VTMOS to the reduced graphene oxide (rGO) surface. The ^{13}C solution

NMR data (B_0 = 7.05 T, without ^1H decoupling during acquisition) for the VTMOS monomer

shows three clearly resolved resonances; a quartet at 47 ppm derived from the methoxy group ($^1J_{CH}$ = 148 Hz), a doublet at 125 ppm from vinyl CH resonance ($^1J_{CH}$ = 145 Hz), and a triplet at 134 ppm corresponding to the terminal CH_2 of the vinyl group ($^1J_{CH}$ = 153 Hz), see Figure 8 (a). The analogous ^{29}Si solution NMR data (B_0 = 7.05 T, without ^1H decoupling during acquisition) exhibits a single T_0 resonance at −57 ppm, Figure 9 (b). The T environments represent the number of oxygen nuclei attached to a silicon environment forming either mono (M), di (D), tri (T) or tetra (Q) silanol bonds, with the subscript corresponding to the number of mono-, di-, tri-substituted siloxane bonds (hence X_n, where X= M, D, T or Q and n= 0,1, 2, 3) [37]. The solid-state ^{13}C MAS NMR spectrum of graphene oxide (GO) presented in Figure 8(c) (B_0 = 7.05 T, ^1H decoupled) shows a series of surface terminate oxygen functional groups and a broad bulk sp^2 hybridized graphene resonance (δ_{iso} = 130 ppm), which have been previously assigned in the literature[17, 43].

After functionalisation of GO with VTMOS, the ^{13}C NMR in Figure 8(d) showed similar peaks to that of GO where both the carbonyl peaks (δ_{iso} = 61.50-71.76 ppm) and the bulk sp^2 hybridized graphene resonance (δ_{iso} = 127.21-137.32 ppm) remained. The presence of the vinyl peak (δ_{iso} = 132.02 (CH) and 130.17 (CH_2) ppm) showed the successful grafting of the silane moiety with the graphene surface. Furthermore, the ^{29}Si spectrum of VTMOS-GO in Figure 8(e) shows traces of T_1 structures and significant increase in T_2 and T_3 structures relative to the T_0 structure seen for VTMOS in Figure 8b.

Despite the intrinsic quantitative nature of the NMR experiment, there are inherent difficulties in quantifying the number of active surface sites compared to the bulk graphene due to the paramagnetic nature of graphene, which can cause signal quenching. Hence, those species proximate to a paramagnetic center will be broadened significantly. The quenching is a result of

the electron-nuclear dipolar coupling which stimulates vastly increased relaxation rates, thus broadening the NMR signal beyond the detection limit of typical solid-state NMR experiments.

The reduction of the graphene oxide (GO) surface and addition of VTMOS causes significant changes in the solid-state ^{13}C MAS NMR spectrum as shown in Figure 8(f). A complete removal of the carboxylic, hydroxyl and ether species suggest that efficient reduction of the graphene oxide (GO) has occurred thus producing a 'clean' graphene surface relative to GO and VTMOS-GO. The presence of ^{13}C vinyl (δ_{iso} = 130 (CH) and 135 (CH$_2$) ppm) and methyl (δ_{iso} = 3 ppm) resonances in the spectrum indicates that chemical interaction of VTMOS with the graphene surface has been achieved. These significantly broader VTMOS resonances in comparison to their ^{13}C solution NMR counterparts (see Figure 8(a)) provide direct evidence that VTMOS has been grafted onto the graphene surface. The increased linewidths observed in the solid-state measurements emanate from reduced/hindered mobility of the VTMOS on the graphene surface, which would introduce a stronger ^{1}H-^{13}C hetero-nuclear dipolar interaction, and from some chemical shift dispersion from disorder on the graphene surface.

There is an approximate 2:1 ratio between the vinyl groups and the methoxy end group, suggesting that some degree of VTMOS polymerization has occurred to form a low molecular weight polymer. Whilst, the sp^2 hybridized graphitic region (Figure 8f)) can be deconvoluted into two regions (δ_{cg} = 161 and 122 ppm), neither coincide with the sp^2 hybridized shift in the graphene oxide (GO) spectrum (δ_{cg} =130 ppm). These two resonances are assigned to graphitic sites that are in close proximity to the grafted VTMOS groups, and form more isolated and unperturbed graphene regions. The resonance at 122 ppm gives a good agreement with the ^{13}C experimental measurements previously achieved on graphene (reduced from graphene oxide)[17, 44].

The corresponding ^{29}Si spectrum of the VTMOS-rGO system (see Figure 8(g)) shows three broad resonances which are assigned to the T_1, T_2 and T_3 silicon environments grafted to the GO[45]. The comprehensive removal of the T_0 resonances from the starting monomer shows that compete grafting of the polymer to the GO has taken place. The presence of T_1, T_2 and T_3 species shows that VTMOS 'polymer' has a range of lengths, as the T_1 and T_2 would give monomers and dimers exclusively, whilst the T_3 site is expected from trimeric (and larger) structures.
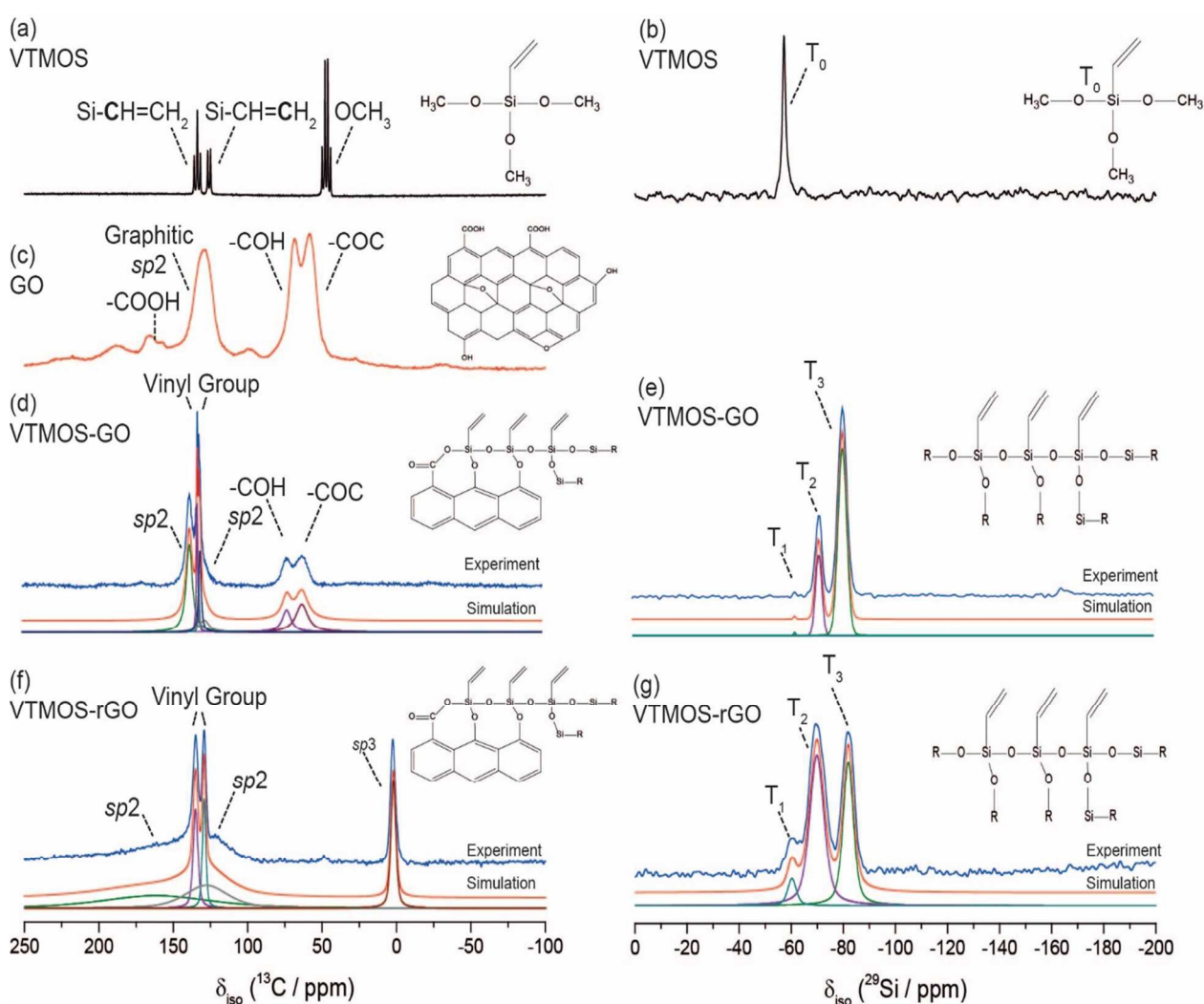
Figure 8. Solution state ^{13}C (a) and ^{29}Si (b) NMR data from VTMOS (B_0 = 7.05 T) compared and contrasted with solid-state ^{13}C MAS NMR data from GO (c), the ^{13}C MAS NMR (d) and (e) ^{29}Si MAS NMR data from the hybrid VTMOS-GO system (v_r = 12 kHz, B_0 = 7.05 T in each case) and the ^{13}C MAS NMR (f) and (g) ^{29}Si MAS NMR data from the hybrid VTMOS-rGO system (v_r = 12 kHz, B_0 = 7.05 T in each case). The simulation of these VTMOS-rGO data is given below each MAS NMR spectrum.

The thermal stability of VTMOS-rGO was measured using TGA and compared to GNPs, GO, VTMOS and VTMOS-GO, see Figure 9. For GO, two major decomposition pathways were observed, firstly at 55°C corresponding to evaporation of water and second at 209°C corresponding to the degradation of carbonyl groups. Like GO, VTMOS was also not thermally stable and started to degrade shortly after it was heated from RT. When GO was functionalised with VTMOS, the thermal degradation of the carbonyls was delayed until ~150°C due to the grafting of the silane however, after continuous heating it degraded rapidly. However, for VTMOS grafted with GO and reduced to VTMOS-rGO, the thermal stability was significantly increased. As shown in Figure 9, there is only one degradation pathway for VTMOS-rGO having an onset of degradation at 590°C corresponding to the oxidative thermal decomposition of the silane grafted to graphene[46]. The thermal stability of rGO is derived from the complete reduction of the hydroxyl groups and the grafting of the carbonyl groups with the silane network. As silicon has lower surface energy, the Si-O-Si network formed would be expected to migrate to the char surface forming a protective layer that prevents further degradation at higher temperatures[47].
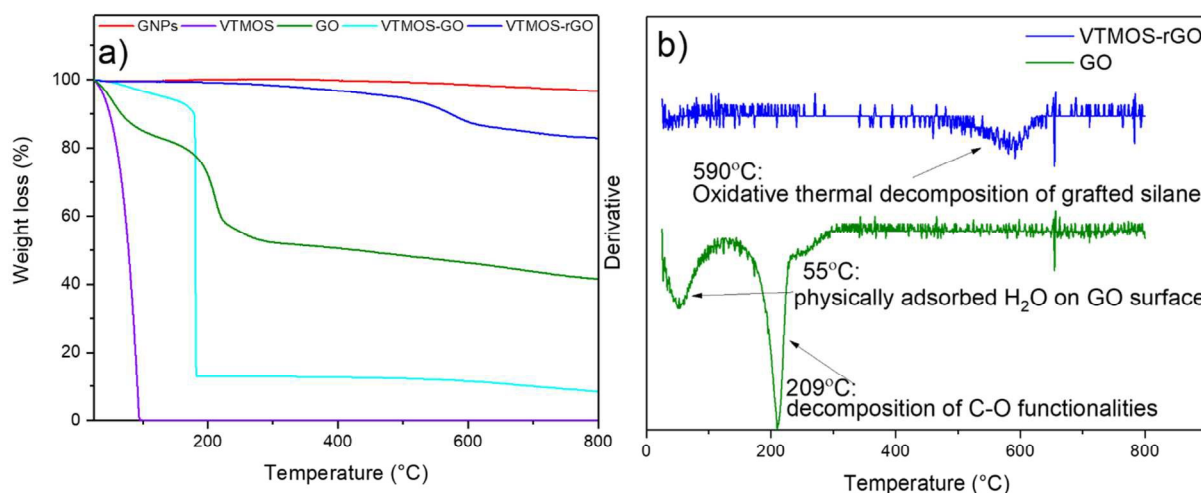
Figure 9. a) TGA (weight loss as a function of temperature) of VTMOS-rGO, GO, VTMOS and GNPs, respectively and b) DTG curves for GO and VTMOS-rGO.

The effect of silane functionalisation on the DC electrical conductivity of VTMOS-rGO was determined using a two-point probe method to measure the electrical resistance of each sample. The resistivity was then determined using $\rho = R\,\frac{A}{l}$ (1), where, ρ is resistivity (Ωm), R is resistance, A is area (m^2) of the test specimen produced and l is length (m) of these sample. The electrical conductivity, σ (Sm)$^{-1}$ was calculated taking the inverse of ρ, according to the relationship- $\sigma = \frac{1}{\rho}$.

The electrical conductivity (Sm^{-1}) of GNPs, GO and VTMOS-rGO was measured as 1.45 Sm^{-1}, 6.72 x 10^{-7} Sm^{-1} and 0.040 Sm^{-1}, respectively. Graphene has planar and hexagonal structures with alternating single and double carbon bonds causing delocalisation of sp^2 carbon electrons that allows zero band gap energy giving rise to the highest relative conductivity. Due to the various hydroxyls and carbonyls present on GO, this planar structure is distorted and causes hindrance to the delocalisation of electrons, resulting in lower electrical conductivity compared

to GNPs. The significant increase in electrical conductivity for VTMOS-rGO relative to GO is attributed to the reduction reaction by hydrazine that retained sp^2 hybridisation. VTMOS-rGO consists of both sp^2 domains and point defects of non-conducting GO areas therefore, electrons can hop from one sp^2 domain to another resulting in flow of current[48]. Additionally, the increase in σ can also attributed to the successful grafting of the silane precursor within graphene sheets followed by the reduction reaction. However, the electrical conductivity of VTMOS-rGO is still lower than that of the GNPs due to the bulky silane spheres located within the graphene sheets causing band gap opening[49].

4. Conclusions

VTMOS-rGO was readily synthesized using a facile approach using an aqueous media *via* an acid-base reaction. The disappearance of the peak in the FTIR spectrum associated with GO hydroxyl groups confirmed complete reduction of modified GO to rGO. Furthermore, the detection of C-O-Si bonding by both FTIR and XPS verified the grafting of rGO with the silane agent and, evidence from Raman spectroscopy confirmed a higher density of defect sites on GO as a consequence of the grafting reaction. SEM images showed the distribution of silane spheres on the rGO surface and within the inter-galley space of GO sheets, which also aided exfoliation of the GO layers. From solid-state NMR measurements, C and Si environments were deduced which supported the T_1, T_2 and T_3 chemical structure of the silane spheres. The grafted VTMOS-rGO network had significantly improved thermal stability and electrical conductivity relative to neat GO. The silane networks are efficient spacers between the rGO layers and will be useful in increasing compatibility with and assisting dispersion of rGO when blended with polymers. Moreover and most critically, the pendant unreacted vinyl groups of the silane provides a route

to crosslinking the silane-rGO network structure to other moieties. This includes grafting the

modified 2D nanofiller with various polymer matrices to promote interfacial interactions

between both phases which will be reported in future publications.

Acknowledgements

References

1.   Hu, H.; Chen, G., Electrochemically modified graphite nanosheets and their nanocomposite films with poly(vinyl alcohol). *Polym. Compos.* **2010,** *31* (10), 1770-1775.

2.   Compton, O. C.; Jain, B.; Dikin, D. A.; Abouimrane, A.; Amine, K.; Nguyen, S. T., Chemically Active Reduced Graphene Oxide with Tunable C/O Ratios. *ACS Nano* **2011,** *5* (6), 4380-4391.

3.   Zhang, J.; Xu, Y.; Cui, L.; Fu, A.; Yang, W.; Barrow, C.; Liu, J., Mechanical properties of graphene films enhanced by homo-telechelic functionalized polymer fillers via π–π stacking interactions. *Composites Part A* **2015,** *71*, 1-8.

4.   Chen, H.; Müller, M. B.; Gilmore, K. J.; Wallace, G. G.; Li, D., Mechanically Strong, Electrically Conductive, and Biocompatible Graphene Paper. *Adv. Mater.* **2008,** *20* (18), 3557-3561.

5.   Lee, C.; Wei, X.; Kysar, J. W.; Hone, J., Measurement of the Elastic Properties and Intrinsic Strength of Monolayer Graphene. *Science* **2008,** *321* (5887), 385-388.

6.   Rohini, R.; Katti, P.; Bose, S., Tailoring the interface in graphene/thermoset polymer composites: A critical review. *Polymer* **2015,** *70*, A17-A34.

7.   Liao, L.; Peng, H.; Liu, Z., Chemistry Makes Graphene beyond Graphene. *JACS* **2014,** *136* (35), 12194-12200.

8.   Ferreira, F. V.; Cividanes, L.; Brito, F. S.; de Menezes, B. R. C.; Franceschi, W.; Simonetti, E. A. N.; Thim, G. P., *Functionalizing Graphene and Carbon Nanotubes: A Review.* Springer International Publishing: 2016.

9.   Geim, A. K.; Novoselov, K. S., The rise of graphene. *Nat Mater* **2007,** *6* (3), 183-191.

Nanoscale Accepted Manuscript

10.   Park, H.; Brown, P. R.; Bulović, V.; Kong, J., Graphene As Transparent Conducting Electrodes in Organic Photovoltaics: Studies in Graphene Morphology, Hole Transporting Layers, and Counter Electrodes. *Nano Lett* **2012,** *12* (1), 133-140.

11.   Foster, C.; P. Down, M.; Zhang, Y.; Ji, X.; Rowley-Neale, S.; Smith, G.; J. Kelly, P.; Banks, C., *3D Printed Graphene Based Energy Storage Devices*. 2017; Vol. 7, p 42233.

12.   Sun, X.; Liu, Z.; Welsher, K.; Robinson, J. T.; Goodwin, A.; Zaric, S.; Dai, H., Nano-Graphene Oxide for Cellular Imaging and Drug Delivery. *Nano Res.* **2008,** *1* (3), 203-212.

13.   Yang, K.; Zhang, S.; Zhang, G.; Sun, X.; Lee, S.-T.; Liu, Z., Graphene in Mice: Ultrahigh In Vivo Tumor Uptake and Efficient Photothermal Therapy. *Nano Lett* **2010,** *10* (9), 3318-3323.

14.   Potts, J. R.; Dreyer, D. R.; Bielawski, C. W.; Ruoff, R. S., Graphene-based polymer nanocomposites. *Polymer* **2011,** *52* (1), 5-25.

15.   Kasaliwal, G. R.; Villmow, T.; Pegel, S.; Pötschke, P., 4 - Influence of material and processing parameters on carbon nanotube dispersion in polymer melts. In *Polymer–Carbon Nanotube Composites*, Woodhead Publishing: 2011; pp 92-132.

16.   Konios, D.; Stylianakis, M. M.; Stratakis, E.; Kymakis, E., Dispersion behaviour of graphene oxide and reduced graphene oxide. *J. Colloid Interface Sci.* **2014,** *430*, 108-112.

17.   Thomas, H. R.; Day, S. P.; Woodruff, W. E.; Vallés, C.; Young, R. J.; Kinloch, I. A.; Morley, G. W.; Hanna, J. V.; Wilson, N. R.; Rourke, J. P., Deoxygenation of Graphene Oxide: Reduction or Cleaning? *Chem. Mater.* **2013,** *25* (18), 3580-3588.

18.   Antonucci, J. M.; Dickens, S. H.; Fowler, B. O.; Xu, H. H. K.; McDonough, W. G., Chemistry of Silanes: Interfaces in Dental Polymers and Composites. *Journal of Research of the National Institute of Standards and Technology* **2005,** *110* (5), 541-558.

19.   Ahmadi, A.; Ramezanzadeh, B.; Mahdavian, M., Hybrid silane coating reinforced with silanized graphene oxide nanosheets with improved corrosion protective performance. *RSC Adv.* **2016,** *6* (59), 54102-54112.

20.   Haeri, S. Z.; Asghari, M.; Ramezanzadeh, B., Enhancement of the mechanical properties of an epoxy composite through inclusion of graphene oxide nanosheets functionalized with silica nanoparticles through one and two steps sol-gel routes. *Prog. Org. Coat.* **2017,** *111* (Supplement C), 1-12.

21.   Xu, P.; Yan, X.; Cong, P.; Zhu, X.; Li, D., Silane coupling agent grafted graphene oxide and its modification on polybenzoxazine resin. *Compos. Interfaces* **2017,** *24* (7), 635-648.

22.   Lee, C. Y.; Bae, J.-H.; Kim, T.-Y.; Chang, S.-H.; Kim, S. Y., Using silane-functionalized graphene oxides for enhancing the interfacial bonding strength of carbon/epoxy composites. *Composites Part A* **2015,** *75* (Supplement C), 11-17.

23.   Pourhashem, S.; Rashidi, A.; Vaezi, M. R.; Bagherzadeh, M. R., Excellent corrosion protection performance of epoxy composite coatings filled with amino-silane functionalized graphene oxide. *Surf. Coat. Technol.* **2017,** *317* (Supplement C), 1-9.

24.   Wang, X.; Xing, W.; Zhang, P.; Song, L.; Yang, H.; Hu, Y., Covalent functionalization of graphene with organosilane and its use as a reinforcement in epoxy composites. *Compos. Sci. Technol.* **2012,** *72* (6), 737-743.

25.   Lee, C. Y.; Le, Q. V.; Kim, C.; Kim, S. Y., Use of silane-functionalized graphene oxide in organic photovoltaic cells and organic light-emitting diodes. *PCCP* **2015,** *17* (14), 9369-9374.

26.   Wan, Y.-J.; Gong, L.-X.; Tang, L.-C.; Wu, L.-B.; Jiang, J.-X., Mechanical properties of epoxy composites filled with silane-functionalized graphene oxide. *Composites Part A* **2014,** *64* (Supplement C), 79-89.

Nanoscale Accepted Manuscript

27.   Pourhashem, S.; Vaezi, M. R.; Rashidi, A.; Bagherzadeh, M. R., Distinctive roles of silane coupling agents on the corrosion inhibition performance of graphene oxide in epoxy coatings. *Prog. Org. Coat.* **2017,** *111* (Supplement C), 47-56.

28.   Ramezanzadeh, B.; Haeri, Z.; Ramezanzadeh, M., A facile route of making silica nanoparticles-covered graphene oxide nanohybrids (SiO2-GO); fabrication of SiO2-GO/epoxy composite coating with superior barrier and corrosion protection performance. *Chem. Eng. J.* **2016,** *303* (Supplement C), 511-528.

29.   Haeri, S. Z.; Ramezanzadeh, B.; Asghari, M., A novel fabrication of a high performance SiO2-graphene oxide (GO) nanohybrids: Characterization of thermal properties of epoxy nanocomposites filled with SiO2-GO nanohybrids. *J. Colloid Interface Sci.* **2017,** *493* (Supplement C), 111-122.

30.   Pourhashem, S.; Vaezi, M. R.; Rashidi, A., Investigating the effect of SiO2-graphene oxide hybrid as inorganic nanofiller on corrosion protection properties of epoxy coatings. *Surface & Coatings Technology* **2017,** *311*, 282-294.

31.   Stöber, W.; Fink, A.; Bohn, E., Controlled growth of monodisperse silica spheres in the micron size range. *J. Colloid Interface Sci.* **1968,** *26* (1), 62-69.

32.   Pleuddemann, E. P., *Silane Coupling Agents*. SECOND EDITION ed.; PLENUM PRESS: NEW YORK AND LONDON, 1991.

33.   Wu, G.; Ma, L.; Liu, L.; Chen, L.; Huang, Y., Preparation of SiO2–GO hybrid nanoparticles and the thermal properties of methylphenylsilicone resins/SiO2–GO nanocomposites. *Thermochim. Acta* **2015,** *613* (Supplement C), 77-86.

34.   Lee, Y.-G.; Park, J.-H.; Oh, C.; Oh, S.-G.; Kim, Y. C., Preparation of Highly Monodispersed Hybrid Silica Spheres Using a One-Step Sol−Gel Reaction in Aqueous Solution. *Langmuir* **2007,** *23* (22), 10875-10878.

35.   Arkhireeva, A.; Hay, J. N., Synthesis of sub-200 nm silsesquioxane particles using a modified Stober sol-gel route. *J. Mater. Chem* **2003,** *13* (12), 3122-3127.

36.   Ahmed, G. S.; Gilbert, M.; Mainprize, S.; Rogerson, M., FTIR analysis of silane grafted high density polyethylene. *Plastics, Rubber and Composites* **2009,** *38* (1), 13-20.

37.   Clemons, C. M.; Sabo, R. C.; Hirth, K. C., The effects of different silane crosslinking approaches on composites of polyethylene blends and wood flour. *J. Appl. Polym. Sci.* **2011,** *120* (4), 2292-2303.

38.   Guan, L.-Z.; Gao, J.-F.; Pei, Y.-B.; Zhao, L.; Gong, L.-X.; Wan, Y.-J.; Zhou, H.; Zheng, N.; Du, X.-S.; Wu, L.-B.; Jiang, J.-X.; Liu, H.-Y.; Tang, L.-C.; Mai, Y.-W., Silane bonded graphene aerogels with tunable functionality and reversible compressibility. *Carbon* **2016,** *107* (Supplement C), 573-582.

39.   Haghdadeh, P.; Ghaffari, M.; Ramezanzadeh, B.; Bahlakeh, G.; Saeb, M. R., The role of functionalized graphene oxide on the mechanical and anti-corrosion properties of polyurethane coating. *Journal of the Taiwan Institute of Chemical Engineers* **2018,** *86*, 199-212.

40.   Guo, X.; Liu, X.; Xu, B.; Dou, T., Synthesis and characterization of carbon sphere-silica core–shell structure and hollow silica spheres. *Colloids Surf., A* **2009,** *345* (1), 141-146.

41.   Childres, I.; Jauregui, L. A.; Park, W.; Caoa, H.; Chena, Y. P., Raman Spectroscopy of Graphene and Related Materials. In *In New Developments in Photon and Materials Research*, Jang, J. I., Ed. Nova Science Publishers: 2013; pp 403-418.

42.   Li, W.; Tang, X.-Z.; Zhang, H.-B.; Jiang, Z.-G.; Yu, Z.-Z.; Du, X.-S.; Mai, Y.-W., Simultaneous surface functionalization and reduction of graphene oxide with octadecylamine for electrically conductive polystyrene composites. *Carbon* **2011,** *49* (14), 4724-4730.

43.   Park, S.; Hu, Y.; Hwang, J. O.; Lee, E.-S.; Casabianca, L. B.; Cai, W.; Potts, J. R.; Ha, H.-W.; Chen, S.; Oh, J., Chemical structures of hydrazine-treated graphene oxide and generation of aromatic nitrogen doping. *Nature communications* **2012,** *3*, 638.

44.   Stankovich, S.; Dikin, D. A.; Piner, R. D.; Kohlhaas, K. A.; Kleinhammes, A.; Jia, Y.; Wu, Y.; Nguyen, S. T.; Ruoff, R. S., Synthesis of graphene-based nanosheets via chemical reduction of exfoliated graphite oxide. *Carbon* **2007,** *45* (7), 1558-1565.

45.   Mahony, O.; Yue, S.; Turdean-Ionescu, C.; Hanna, J. V.; Smith, M. E.; Lee, P. D.; Jones, J. R., Silica–gelatin hybrids for tissue regeneration: inter-relationships between the process variables. *J. Sol-Gel Sci. Technol.* **2014,** *69* (2), 288-298.

46.   Ramezanzadeh, B.; Ahmadi, A.; Mahdavian, M., Enhancement of the corrosion protection performance and cathodic delamination resistance of epoxy coating through treatment of steel substrate by a novel nanometric sol-gel based silane composite film filled with functionalized graphene oxide nanosheets. *Corros. Sci.* **2016,** *109* (Supplement C), 182-205.

47.   Chiang, C. L.; Yang, J. M., 10 - Flame retardance and thermal stability of polymer/graphene nanosheet oxide composites. In *Fillers and Reinforcements for Advanced Nanocomposites*, Woodhead Publishing: 2015; pp 253-272.

48.   Junsheng, M.; Xueyan, H.; Mingpeng, Y.; Jingzheng, H.; Xinyu, R.; Hong, Q.; Rongming, W., Functional chemically modified graphene film: microstructure and electrical transport behavior. *J. Phys. D: Appl. Phys.* **2017,** *50* (43), 435101.

49.   Deka, M. J.; Baruah, U.; Chowdhury, D., Insight into electrical conductivity of graphene and functionalized graphene: Role of lateral dimension of graphene sheet. *Mater. Chem. Phys.* **2015,** *163* (Supplement C), 236-244.